from 20 to 25% (VSWR < 2). For a stub width W of 3 mm, an increase in the stub length L results in another higher frequency resonant point at 4.5 GHz. For a stub width W of 4 and 5 mm, the return loss between two resonant points further decreases, and results in the wide impedance bandwidth, which can be more than 40% for a stub length L of 14 mm. However, when the stub width increases to 6 or 7 mm, the lower resonant frequency point becomes quite high, and the impedance bandwidth decreases.

Figure 9 shows the radiation patterns of the proposed antenna. From the two copolarization patterns, the front-to-back ratio is noted to be unity. As the space wave in the vicinity of the truncated ground plane is stronger in the E-plane, it suffers from a greater diffraction than the H-plane. The measured cross-polarization level in the E-plane usually is less than -15 dB, while in the H-plane, the cross-polarization is more than -10 dB in the range of $\pm 30°$.

The current plot at 3.5 GHz is depicted in Figure 10. As shown in the figure, the copolarization is predicted to be low as there is relatively no current on the lateral side of the antenna.

CONCLUSIONS

A novel wide slot antenna fed by CPW realized on a substrate with a high dielectric constant is presented. The antenna has a simple geometry. Through the adjustment of the width and length of the stub, good impedance matching of more than 40% bandwidth can be achieved. This kind of antenna can be integrated easily with other active devices without any external balun network.

REFERENCES

1. E.A. Soliman, S. Brebels, P. Delmotte, G.A.E. Vandenbosch, and E. Beyne, Bow-tie slot antenna fed by CPW, Electron Lett 35 (1999), 514–515.
2. X. Ding and A.F. Jacob, CPW-fed slot antenna with wide radiating apertures, Proc Inst Elect Eng 145 (1998).
3. J.F. Huang and C.W. Kuo, CPW-fed bow-tie slot antenna, Microwave Opt Technol Lett 19 (1998).

ACCURATE COMPUTATION OF A CIRCULAR-DISK PRINTED ANTENNA AXISYMMETRICALLY EXCITED BY AN ELECTRIC DIPOLE

Natalia Yu. Bliznyuk,[1] Alexander I. Nosich,[1] and Alexander N. Khizhnyak[2]

[1] Institute of Radiophysics and Electronics
National Academy of Sciences
Kharkov 310085, Ukraine
[2] Kharkov State Academy of Civil Engineering
Kharkov 310002, Ukraine

Received 29 November 1999

ABSTRACT: *Galerkin's method, combined with the method of analytical regularization in the Hankel-transform domain, is used to analyze a circular-disk metallic printed antenna. The fundamental effects are investigated, such as the surface-wave and space-wave powers and the radiation efficiency. The validity of the cavity (magnetic-current) model is studied.* © 2000 John Wiley & Sons, Inc. Microwave Opt Technol Lett 25: 211–216, 2000.

Key words: *microstrip antenna; surface waves; radiation efficiency; cavity model*

I. INTRODUCTION

The practical advantages of microstrip antennas are now well known, and have been discussed in many papers. The published literature contains numerous analyses of various radiating printed elements performed by the approximate circuit-theory and cavity-model methods [1], full-wave methods such as Galerkin's method in the space- and Hankel-transform domains [2, 3], and the mixed-potential integral-equation (MPIE) method [4].

The aim of this paper is to present an efficient solution to the diffraction problem for a circular metallic patch (see Fig. 1) based on the method of analytical regularization (MAR). Here, MAR exploits an explicit inversion of the singular part of the corresponding full-wave dual-integral equations in the transform domain [5]. A numerical algorithm based on the MAR outperforms conventional moment-method algorithms due to a much smaller matrix size and few numerical integrations for filling the matrix, and has a controlled accuracy.

II. PROBLEM FORMULATION

Consider the geometrical configuration shown in Figure 1: a metallic circular disk of zero thickness, separated from the ground plane by a dielectric substrate of thickness h and permittivity ε. We assume that this structure is excited by a vertical electrical dipole (VED) located on the ground plane. Such a source simulates a coaxial probe feed. The origin of the coordinate system is chosen at the dipole. The disk and ground plane are assumed to be perfectly electric conducting (PEC), the substrate and the ground plane being infinite. All geometrical and wavelength parameters are dimensionless and normalized by the disk radius a.

The total electromagnetic field $\{\mathbf{E}, \mathbf{H}\}$ must satisfy the Maxwell equations in the layered medium, the tangential-component continuity at the dielectric surface, the PEC boundary conditions on the disk and the ground plane, a modified radiation condition, which takes into account the presence of the surface waves, and the edge condition on the disk rim.

We assume time dependence in the form $e^{i\omega t}$. As we consider a VED located at the origin of the spherical and cylindrical coordinates $\{R, \varphi, \theta\}$ and $\{\rho, \varphi, z\}$, the driving electric current is

$$J_z^e = I^e l \frac{\delta(\rho' - 0)}{\rho'} \delta(\varphi' - 0) \delta(z' - 0). \qquad (1)$$

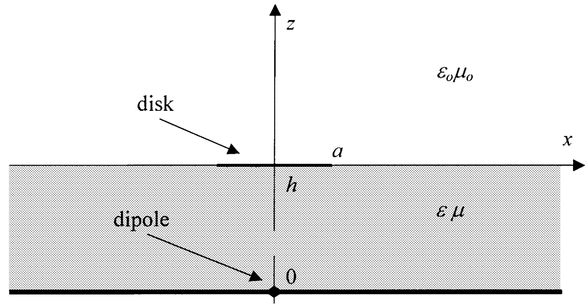

Figure 1 Cross-sectional view of the problem geometry

The field components generated by such a current are φ independent due to the axial symmetry of both the geometry and the excitation. Now, we split the total field into an incident one and one scattered by the disk. The incident field is considered to be that of the PEC-grounded substrate with a VED excitation (i.e., in the absence of a disk). The expressions for this field have been obtained, and its properties have been studied in [6]. Thereby, the total electromagnetic field components in the free half-space and in the substrate, respectively, are sought in the form of the following Hankel transforms:

$$
\begin{aligned}
E_\rho^0 &= \frac{1}{i\omega\varepsilon_0}\int_0^\infty J_1(\kappa\rho)F^0 e^{-\gamma_0 z}\kappa^2\,d\kappa \\
E_z^0 &= \frac{1}{i\omega\varepsilon_0}\int_0^\infty J_0(\kappa\rho)F^0 e^{-\gamma_0 z}\frac{\kappa^3}{\gamma_0}\,d\kappa \\
H_\varphi^0 &= \int_0^\infty J_1(\kappa\rho)F^0 e^{-\gamma_0 z}\frac{\kappa^2}{\gamma_0}\,d\kappa
\end{aligned} \tag{2}
$$

and

$$
\begin{aligned}
E_\rho^\varepsilon &= -\frac{1}{i\omega\varepsilon}\int_0^\infty J_1(\kappa\rho)[F^+ e^{\gamma_\varepsilon z} - F^- e^{-\gamma_\varepsilon z}]\kappa^2\,d\kappa \\
E_z^\varepsilon &= \frac{1}{i\omega\varepsilon}\int_0^\infty J_0(\kappa\rho)[F^+ e^{\gamma_\varepsilon z} + F^- e^{-\gamma_\varepsilon z}]\frac{\kappa^3}{\gamma_\varepsilon}\,d\kappa \\
H_\varphi^\varepsilon &= \int_0^\infty J_1(\kappa\rho)[F^+ e^{\gamma_\varepsilon z} + F^- e^{-\gamma_\varepsilon z}]\frac{\kappa^2}{\gamma_\varepsilon}\,d\kappa
\end{aligned} \tag{3}
$$

where

$$F^0 = f_0^0 + f_s^0,\; F^+ = f_0^+ + f_s^\varepsilon,\; F^- = f_0^- + f_s^\varepsilon \tag{4}$$

$$f_0^0 = \frac{Il}{2\pi}\frac{\gamma_0}{D_m(\kappa)}e^{\gamma_0 h},\; f_0^\pm = \frac{Il}{4\pi}\frac{\gamma_\varepsilon \mp \varepsilon\gamma_0}{D_m(\kappa)}e^{\mp\gamma_\varepsilon h} \tag{5}$$

$$D_m(\kappa) = \gamma_\varepsilon \sinh(\gamma_\varepsilon h) + \varepsilon\gamma_0\cosh(\gamma_\varepsilon h). \tag{6}$$

Note that (5) and (6) are the known functions, whereas f_s^0 and f_s^ε are the unknown functions, and the indexes 0 and ε refer to the free half-space and the dielectric substrate, respectively.

The boundary and continuity conditions for the total tangential fields in this microstrip structure are

$$[\mathbf{n}, \mathbf{E}^0] = [\mathbf{n}, \mathbf{E}^\varepsilon] = 0, \qquad z = 0,\ \rho \le 1 \tag{7}$$

$$[\mathbf{n}, \mathbf{E}^0 - \mathbf{E}^\varepsilon] = 0, \qquad z = h \tag{8}$$

$$[\mathbf{n}, \mathbf{H}^\varepsilon - \mathbf{H}^\varepsilon] = 0, \qquad z = h,\ \rho > 1. \tag{9}$$

On substituting (2) and (3) into the above conditions and introducing the unknown Hankel transform of the current density on the disk $\alpha(\kappa) = (2f_s^\varepsilon \mathrm{D}_m(\kappa)\kappa^2/\varepsilon\gamma_0\gamma_\varepsilon) = (-f_s^0 e^{-\gamma_0 h} D_m(\kappa)\kappa^2/2\gamma_0\gamma_\varepsilon \sinh\gamma_\varepsilon h)$, we arrive at the set of dual-integral equations (DIE) in the Hankel-transform domain:

$$
\begin{cases}
\int_0^\infty J_1(\kappa\rho)\alpha(\kappa)\,d\kappa = 0, & \rho > 1 \\
\int_0^\infty J_1(\kappa\rho)\beta(\kappa)\alpha(\kappa)\,d\kappa = \int_0^\infty J_1(\kappa\rho)\Pi^0(\kappa)\gamma_0\kappa^2\,d\kappa, \\
\rho \le 1
\end{cases} \tag{10}
$$

where

$$\beta(\kappa) = \frac{\gamma_0\gamma_\varepsilon \sinh(\gamma_\varepsilon h)}{D_m(\kappa)} \tag{11}$$

$$\Pi^0 = \frac{I^e l}{2\pi}\frac{1}{D_m(\kappa)}. \tag{12}$$

Real zeros of the denominator $D_m(\kappa)$ exist in the case of $\operatorname{Im}\varepsilon = 0$. They correspond to the TM surface-wave poles of the lossless substrate.

III. METHOD OF REGULARIZATION

In order to transform the DIE (10) into an infinite matrix equation of the Fredholm second kind that guarantees the convergence of the numerical solution, we discretize the DIE by using a Galerkin projection scheme with a set of judiciously chosen basis functions.

One knows that the unknown function of the current density in the space domain must satisfy the edge condition on the disk rim. As an expansion basis, we use a set of orthogonal functions proposed in [7], which enable satisfying this condition in a term-by-term manner:

$$
\Psi_n(\rho) = \begin{cases}
2^{-1/2}\dfrac{\rho n!}{\Gamma(n+3/2)}\sqrt{4n+5}\,(1-\rho^2)^{1/2} \\
\quad P_n^{(1,1/2)}(1-2\rho^2), & \rho \le 1 \\
0, & \rho > 1
\end{cases} \tag{13}
$$

where $P_n^{(1,1/2)}(x)$ are the Jacobi polynomials. The Hankel transform of (13) is

$$\psi_n(\kappa) = \int_0^\infty \Psi_n(\rho)J_1(\kappa\rho)\rho\,d\rho = \sqrt{4n+5}\,J_{2n+5/2}(\kappa)\kappa^{-1/2}. \tag{14}$$

These functions, which are proportional to the spherical Bessel functions, turn out to be orthogonal on the interval $\kappa \in (0,\infty)$ [8]:

$$\int_0^\infty \psi_n(\kappa)\psi_k(\kappa)\,d\kappa = \delta_{nk}. \tag{15}$$

Now, we expand the unknown function $\alpha(\kappa)$ as

$$\alpha(\kappa) = \sum_{n=0}^\infty x_n\psi_n(\kappa) \tag{16}$$

where x_n are unknown coefficients. Note that such a choice of the basis functions allows satisfaction of the first equation of (10) identically.

Further, we note that, if $ka \to 0$ and $h/a \to \infty$, then $\beta(\kappa) = \kappa + o(\kappa^{-1})$. Therefore, we split the weight function of the second equation of (10) into a static-free-space part and a dynamic-layered-medium part:

$$\beta(\kappa) = \frac{\kappa}{1+\varepsilon}\{1 - \Omega(\kappa)\},$$
$$\Omega(\kappa) = 1 - (1+\varepsilon)\frac{\gamma_0\gamma_\varepsilon \sinh(\gamma_\varepsilon h)}{\kappa D_m(\kappa)}. \quad (17)$$

Here, $\Omega(\kappa) = o(\kappa^{-2})$ as $\kappa \to \infty$. Due to both this extraction and the expansion (16), we can diagonalize and analytically invert the static-free-space part of the second equation of the DIE (10) by using the transform (14) and the property of orthogonality of the Bessel functions (15). On so doing, we obtain an infinite matrix equation for the expansion coefficients:

$$x_k - \sum_{n=0}^{\infty} x_n A_{kn} = B_k \quad (18)$$

where

$$A_{kn} = \int_0^\infty \psi_k(\kappa)\psi_n(\kappa)\Omega(\kappa)\, d\kappa,$$
$$B_k = (1+\varepsilon)\int_0^\infty \psi_k(\kappa)\Pi_0(\kappa)\gamma_0\kappa\, d\kappa. \quad (19)$$

Due to the large-index behavior of the Bessel functions, $\Sigma_{k,n=0}^{\infty}|A_{kn}|^2 < \infty$. Hence, (18) is the second-kind Fredholm equation in the space of the square-summable number sequences L_2.

IV. COMPUTATIONAL ASPECTS

When microstrip structures are considered, many numerical techniques such as FDTD generate very large systems of linear equations. The known numerical solutions and commercial CAD packages based on the integral equations and conventional method-of-moments (MoM) solvers also require significant CPU and memory resources [4]. Moreover, near the sharp resonances, both MOM and FDTD have a well-known loss of accuracy [9]. Our method enables one to noticeably reduce the memory and computation time expenditures due to the much smaller truncated matrix size needed for practical accuracy, and few numerical integrations for filling the matrix. Our algorithm is always stable due to a small variation of the matrix condition number when changing the problem parameters, even in the resonances.

The general theory of matrix equations of the Fredholm second kind shows that the calculation error can be minimized by means of increasing the truncation number N. Figure 2 demonstrates that the normalized truncation error, by the norm in L_2, that is given by

$$\delta(N) = \frac{\sqrt{\sum_{n=0}^{N} |x_n^N - x_n^{N-1}|^2}}{\sqrt{\sum_{n=0}^{N} |x_n^N|^2}}, \quad (20)$$

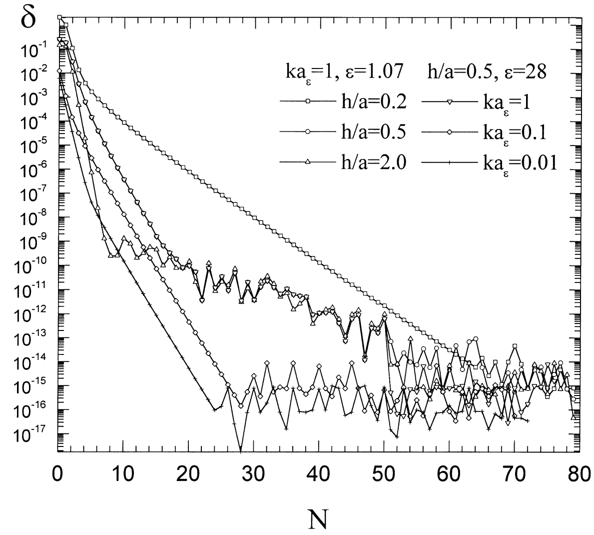

Figure 2 Truncation error

decreases very rapidly with larger N. Further, it depends more on the ratio h/a than on the dielectric constant of the substrate or the electric size of the patch. This is due to extracting and inverting the static-free-space part [see (17)]. If the parameter h/a decreases, the matrix elements in (19) increase since the contribution of the noninverted part of (11) becomes larger.

In general, the integrands of the matrix elements of (19) are functions of the parameter κ, varying on the complex plane with branch points at $\pm ka_0$, cuts, and several real-value poles corresponding to the surface waves. These poles are located on the real κ-axis between ka_0 and $ka_0\sqrt{\varepsilon}$. To compute these integrals, we deform the path Γ as shown in Figure 3. The choice of points A, B, and C is conditioned by the influence of the poles and the properties of the Bessel functions. The upper limit D has been calculated with provision for the condition

$$\int_D^\infty f(ka, \varepsilon, h/a)\kappa^{-m}\, d\kappa < 10^{-15} \quad (21)$$

where m corresponds to the asymptotic behavior of the integrand. In order to increase the power m and, respec-

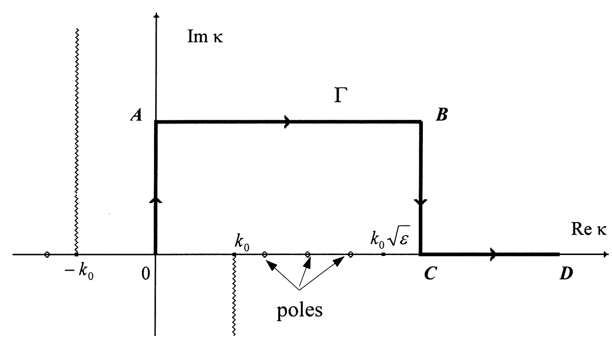

Figure 3 Contour of integration in complex κ-plane

tively, to decrease the interval CD, we extract the first few terms of the expansion of the integrand in terms of the power series of parameter ka/κ, and solve them analytically [8] by the following scheme:

$$\int_0^\infty \psi_k \psi_n \Omega(\kappa)\, d\kappa = \int_0^\infty \psi_k \psi_n \left\{ \Omega(\kappa) - \sum_{j=1}^{m} q_j \left(\frac{ka}{\kappa} \right)^{2j} \right\} d\kappa + \sum_{j=1}^{m} q_j \int_0^\infty \left(\frac{ka}{\kappa} \right)^{2j} \psi_n \psi_k \, d\kappa. \quad (22)$$

In addition, we use the recurrence relations for the Bessel functions, as was proposed in [7], and the fact that $\{A_{kn}\}$ is a symmetric matrix. This enables us to calculate $3N$ instead of N^2 integrals on the left-hand side of (19), where N is the truncation number. Due to the above-mentioned statements, both computer time and memory resources have been decreased approximately in hundred times without a loss of calculation accuracy.

The Poynting theorem in complex form (with the real parts defining the time-averaging power values) was used to obtain a partial validation of the obtained results by checking the power conservation:

$$-\mathrm{Re} \int_{V \to \infty} \mathbf{j}^{e^*} \mathbf{E}\, dv = \mathrm{Re} \int_{S \to \infty} [\mathbf{E}\mathbf{H}^*] \times \mathbf{n}\, ds \quad (23)$$

where S is the surface enclosing a finite volume V. We emphasize that, in all of our computations, the error in (23) was at the level of 10^{-14}.

V. NUMERICAL RESULTS

Based on Eq. (18), we have computed the far-field values of interest, such as the space- and surface-wave powers and the radiation efficiency. All of the calculations have been carried out by following the scheme proposed in [6]. In the figures, all of the power values are normalized to the radiation power of a dipole located on the PEC ground plane in the free half-space:

$$P_{\mathrm{norm}} = \frac{(I^e kl)^2}{6\pi}. \quad (24)$$

The radiation efficiency is defined as

$$\eta = \frac{P_{\mathrm{space}}}{P_{\mathrm{space}} + P_{\mathrm{surface}}}. \quad (25)$$

Figure 4 shows the powers of all types of waves excited in a microstrip antenna, and the radiation efficiency versus the normalized free-space wavelength. In Figure 4(a), the powers of the surface-wave modes are presented. Besides the simultaneous maxima both in the surface- and space-wave powers, like 1 and 7, there are some sharp resonances that also influence the value of the radiation efficiency [see Fig. 4(c)]. So, we can divide these resonances into high-Q and low-Q ones, such as 2, 3, and 1, respectively. Resonance 2 and "antiresonance" 5 are observed in the cases where the new surface waves start propagating. In Figure 4(b), the total power of the surface waves and the space-wave power are shown. The power of the space wave has a significantly lower level than the surface one, except for resonances 2 and 3. In

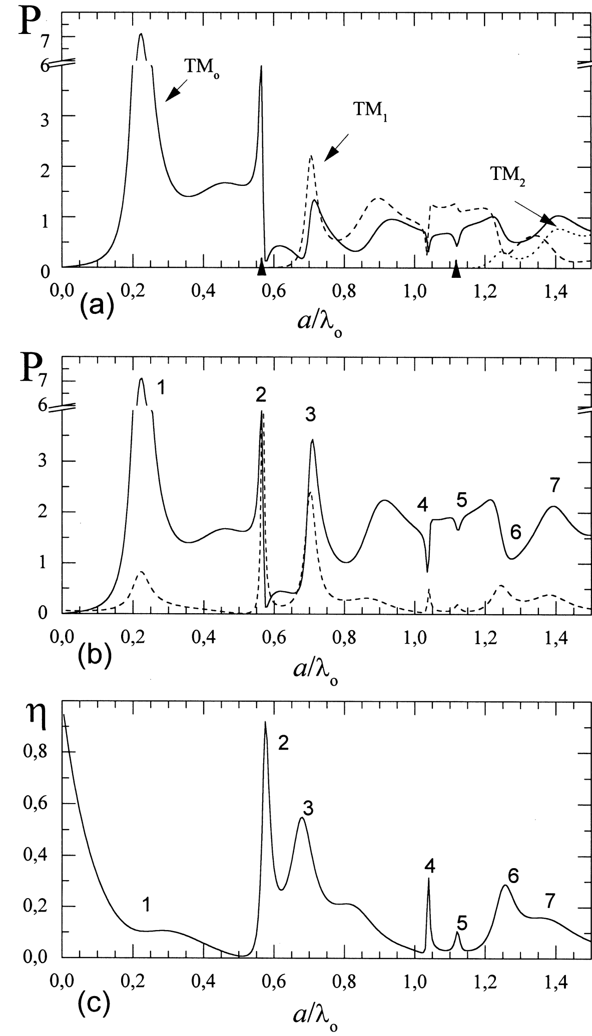

Figure 4 Antenna characteristics versus frequency. $\varepsilon = 4$, $h/a = 0.5$. (a) Powers of the surface waves. (b) Total power of all surface waves (solid line) and the space-wave power (dashed line). (c) Radiation efficiency

Figure 5, the curves of the surface- and space-wave powers and the radiation efficiency versus the normalized free-space wavelength are plotted for different values of the substrate permittivity. As seen, the use of low-permittivity substrates is preferable to achieve a high level of radiation efficiency.

VI. LIMITATIONS AND VALIDITY OF THE CAVITY MODEL

One of our goals was to visualize the validity range of the cavity model frequently used in approximate printed-antenna design [1]. The other goal was to check the widely accepted criterion of minimization of the surface-wave power that is important for increasing the antenna gain and efficiency. According to this model, the magnetic field on the disk rim $\rho = a$ is zero, the electric field is purely transverse, and the electric current on the top surface of the patch is zero as well. Hence, the radiation into the layered half-space results from the magnetic-current ring (MCR) along the disk rim. For thin substrates, the model of a magnetic ring current is usually assumed to be a sufficient approximation. We have found the electromagnetic fields for a PEC-grounded sub-

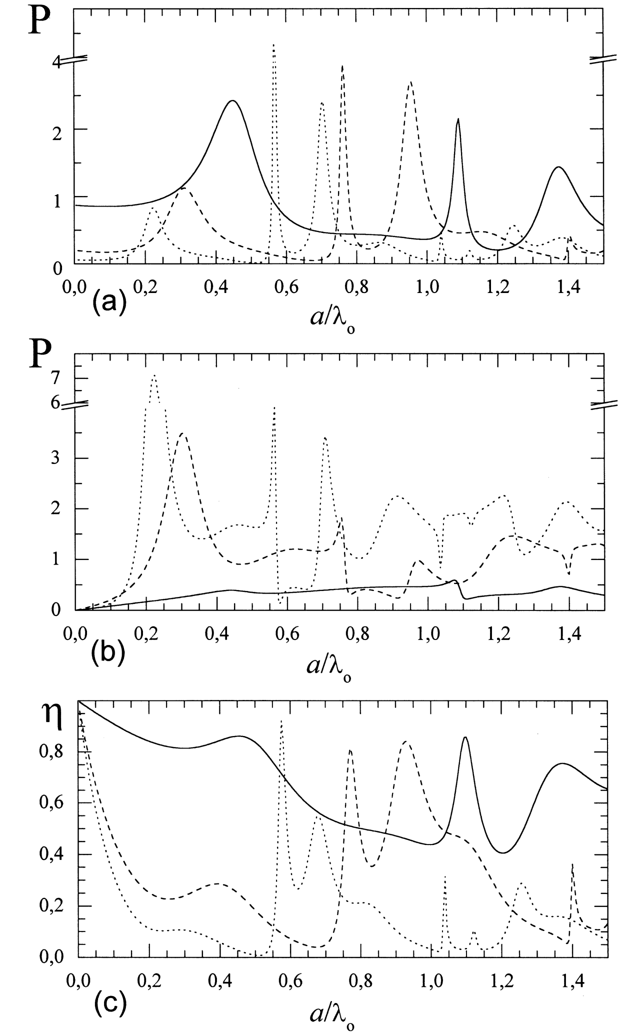

Figure 5 Antenna characteristics versus frequency. $h/a = 0.5$; $\varepsilon = 1.07$, solid lines; $\varepsilon = 2.2$, dashed lines; $\varepsilon = 4$, dotted lines. (a) Power of the space wave. (b) Total power of the surface waves. (c) Radiation efficiency

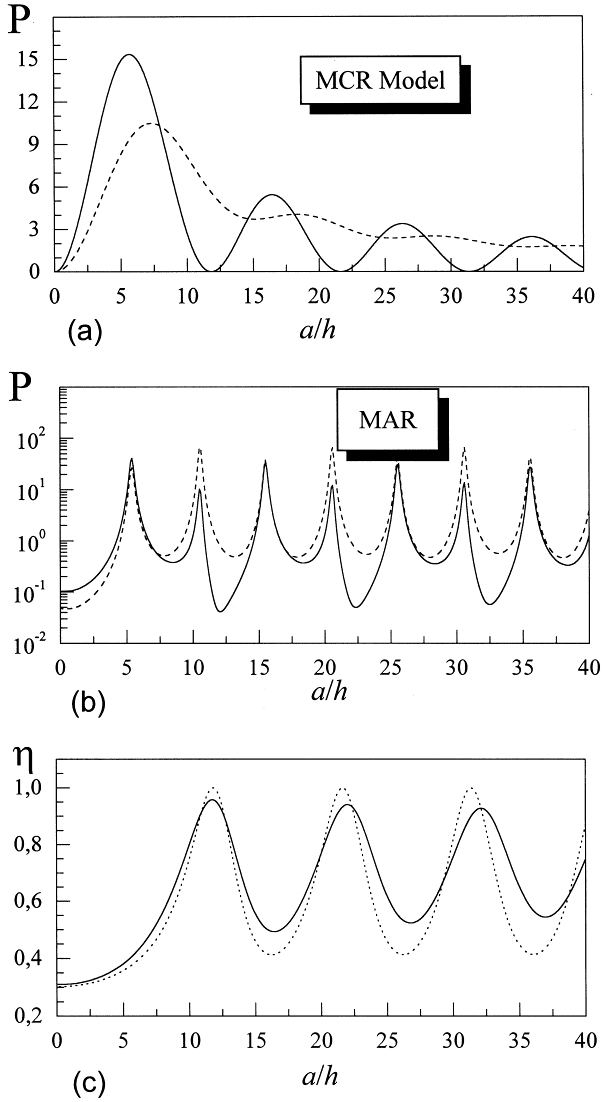

Figure 6 Radiation efficiency and wave powers versus a/h. $\varepsilon = 4$, $a/\lambda_0 = 0.05$. (a)–(b) Surface-wave power (solid lines), space-wave power (dashed lines). (c) Radiation efficiency: MAR (solid line), and MCR (dotted line)

strate assuming that the driving magnetic current is

$$J_{\varphi}^{m} = I^{m}\delta(r' - a)\delta(z' - 0). \tag{26}$$

The expressions for the excited surface wave fields turn out to be proportional to $J_1(\beta_{\mathrm{TM}_n}a)$, where β_{TM_n} is the propagation constant of the TM_n surface wave. Thus, the disk patch antenna will not excite the TM_0 surface wave, provided that the radius of the MCR is chosen to satisfy

$$J_1(\beta_{\mathrm{TM}_0}a) = 0. \tag{27}$$

This brings us to the values of the "no-surface-wave" radius as $\beta_{\mathrm{TM}_0}a = 3.83171, 7.01559, \dots$.

In Figure 6, the space- and surface-wave powers and the radiation efficiency versus the geometrical parameter h/a are presented. As seen, the results obtained by using the MAR and by MCR approximation have a good agreement only for the radiation efficiency. MAR-calculated fields have a more complicated structure: sharp resonances, the maxima of which are observed near the zeros of $J_3(ka_{\varepsilon})$, have nearly equal amplitudes, both in the surface-wave and space-wave powers. Therefore, the resonances do not influence the value of the radiation efficiency. Unlike this, the effect of minimization due to satisfying condition (25) is found for the surface waves exclusively. Physically, if the magnetic component of the surface-wave field is close to zero, a virtual "cavity" with magnetic walls is formed under the patch. It suppresses the surface-wave power, but does not influence the value of the space-wave power. This effect is especially remarkable ($\eta \approx 1$) for thin substrates or for substrates with permittivities. Figure 7 shows the plots obtained by means of MAR and by the MCR approximation for the patch radius corresponding to the first maximum in the radiation efficiency, due to the TM_0 surface-wave suppression. The results are given for different values of the substrate permittivity. As seen, the MCR model can be used for the very thin substrates, and cannot be used for the low-permittivity substrates. Furthermore, it yields no correct information about the true level of the radiation efficiency (if (25) is satisfied, then $\eta = 1$) that is very important for practical applications.

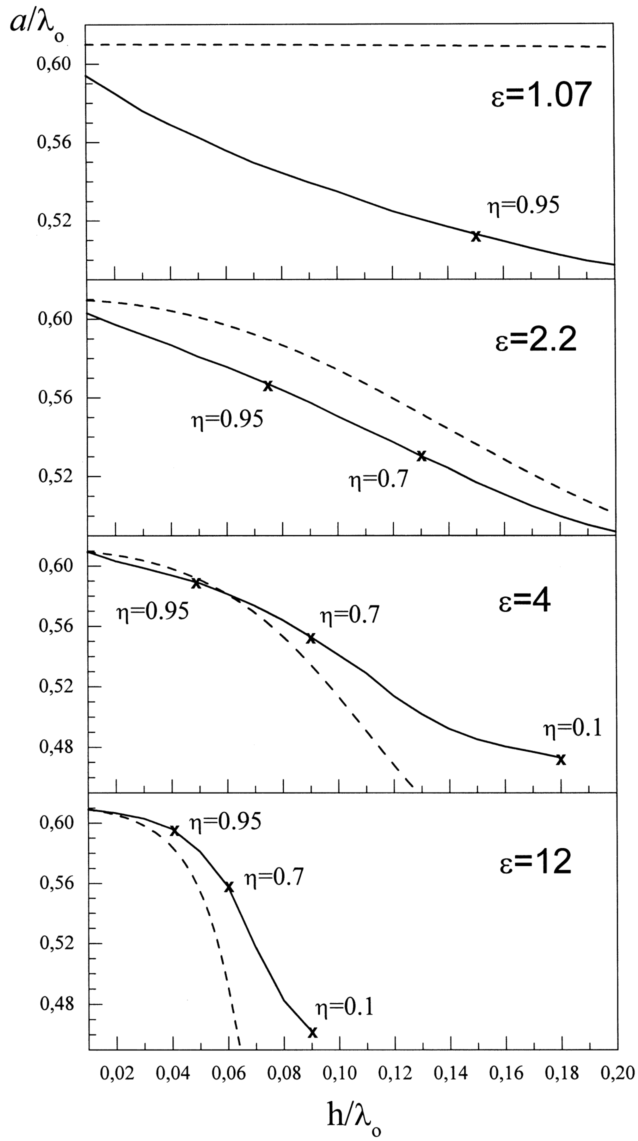

Figure 7 Patch radius versus normalized substrate thickness for a patch radius necessary to suppress the surface-wave excitation in a single-mode operation. MAR, solid lines; MCR model, dashed lines; $h/a = 0.05$

VII. CONCLUSION

The method of analytical regularization combined with the Galerkin method has been proposed to determine the fundamental antenna effects in a circular-disk metallic patch antenna on a dielectric substrate backed by a PEC ground plane and coaxially excited by a vertical electrical dipole. Due to analytical inversion of the free-space static-part operator, the dual-integral equations in the transform domain proved able to be converted into the infinite matrix equation of the Fredholm second kind. This matrix equation has been solved by means of an efficient numerical procedure. Our solution is stable in the resonant region, unlike the conventional MoM ones. Further, this algorithm enables one to significantly reduce the machine time and memory resources.

Antenna characteristics, such as the surface- and space-wave powers and the radiation efficiency, have been obtained and analyzed for different values of the substrate thickness and permittivity, patch radius, and frequency. The resonance conditions have been established as those that maximize radiation power or efficiency. The criteria have been determined for the material properties and dimensions, for which the surface waves are nearly eliminated and the radiation efficiency approaches 100%. A comparison with the magnetic-ring model (i.e., the cavity model applied to compute the radiated field) is given. This approximation has been shown to have a limited range of application: thin and high-contrast dielectric substrates.

REFERENCES

1. R.D. Jackson, J.T. Williams, A.K. Bhattacharyya et al., Microstrip patch designs that do not excite surface waves, IEEE Trans Antennas Propagat 41 (1993), 1026–1037.
2. W.C. Chew and J.A. Kong, Resonances of the axial-symmetric modes in microstrip disk resonators, J Math Phys 21 (1980), 582–591.
3. V. Losada and R.R. Boix, Resonant modes of circular microstrip patches in multilayered substrates, IEEE Trans Antennas Propagat 47 (1999), 448–497.
4. J.R. Mosig, R.C. Hall, and F.E. Gardiol, "Numerical analysis of microstrip patch antennas," Handbook of microstrip antennas, J.R. James and P.S. Hall (Editors), Peter Peregrinus, London, England, 1989, pp. 391–453.
5. A.I. Nosich, MAR in the wave-scattering and eigenvalue problems: Foundations and review of solutions, IEEE Antennas Propagat Mag 42 (1999), 34–49.
6. N.Yu. Bliznyuk and A.I. Nosich, Basic properties of the fields excited by VED and HMD located in a dielectric substrate backed by a perfectly conducting ground plane, Microwave Opt Technol Lett 15 (1997), 316–320.
7. A.N. Khizhnyak, Diffraction of a plane wave by a circular disk, Sov Phys Acoust 35 (1989), 539–541.
8. M. Abramovitz and I.A. Stegun, Handbook of mathematical functions, National Bureau of Standards, Washington, DC, 1964, chap. 10, 11.
9. G.L. Hower, R.G. Olsen, J.D. Earls, and J.B. Schnieder, Inaccuracies in numerical calculation of scattering near natural frequencies of penetrable objects, IEEE Trans Antennas Propagat 41 (1993), 982–986.

DESIGN AND PROTOCOL ANALYSIS FOR PASSIVE STAR TOPOLOGY OF A WDM NETWORK

Ioannis E. Pountourakis[1]
[1] Department of Electrical and Computer Engineering
Division of Computer Science
National Technical University of Athens
157 73 Zographou, Athens, Greece

Received 5 November 1999

ABSTRACT: *In this letter, we study a single-hop network for a passive star topology, where each station communicates with the other by assigning a fixed wavelength to each station. A station transmits its packets to another station by transmitting over its dedicated wavelength. All of these dedicated wavelengths are multiplexed by WDM into a multiwavelength broadcast system. To enable the destination station to know which packets from the WDM system are destined for it, we introduce the multichannel control architecture (MCA). The MCA with an appropriate network interface unit (NIU) at each station gives the solution to the problem of the electronic processing bottleneck that the single common shared control channel for pretransmission coordination introduces. An analytic model is developed and analyzed for performance measures evaluation based on Poisson approximation statistics for finite*